Hidden structure in the medium-range order of amorphous zirconia-tantala films

Alec Mishkin, Jun Jiang, Rui Zhang, Hai-Ping Cheng, Kiran Prasai, Riccardo Bassiri, and Martin Fejer

Phys. Rev. B **108**, 054103 — Published 14 August 2023

DOI: 10.1103/PhysRevB.108.054103

Hidden structure in the medium range order of amorphous zirconia-tantala films

Alec Mishkin, Jun Jiang, Rui Zhang, and Hai-Ping Cheng
Department of Physics and Quantum Theory Project, University of Florida, 2001 Museum Road, Gainesville, Florida 32611, USA

Kiran Prasai, Riccardo Bassiri, and Martin Fejer
E. L. Ginzton Laboratory, Stanford University, Stanford, California 94305, USA
(Dated: July 17, 2023)

Due to both its scale and complexity, medium range order is difficult to study. In this work, we present a new computational tool which identifies the shortest path of bonded atoms which connect any pair of atoms an arbitrary distance apart. We call these atomic structures chains and they are well suited for characterizing medium range order. We apply this tool to Force Enhanced Atomic Refinement produced models of 50% zirconia-tantala. These models show a systematic change in the medium range order caused by heat treatment, which, by using this new tool, we attribute to chains becoming kinkier. We also perform an in-depth analysis on specific chains to demonstrate that peaks seen in the pair distribution function are correlated to each other. Zirconia-tantala is used as an example of the utility of this tool, but we can easily apply it to other materials.

I. INTRODUCTION

A common probe into the atomic structure of amorphous materials is the pair distribution function (PDF). A typical PDF of amorphous materials exhibits sharp peaks in the short range (up to 5 Å) and progressively weaker peaks in the medium range (5 Å to 50 Å). The features in medium range order (MRO) of amorphous films have been shown to correlate with several measured properties of the films including mechanical loss [1], urbach tails [2–5] and Raman features [6, 7]. However, unlike the short range features, which are relatively well understood for most systems and can usually be explained in terms of coordination numbers, bond lengths, bond angles etc., the features in MRO are less well understood.

There are a number of preexisting experimental and computational methods for analyzing MRO of amorphous materials. One such method is fluctuation electron microscopy (FEM) [8], which can also be simulated with atomic models [9]. FEM is well suited for identifying qualitative features of MRO, and has also been used to obtain the general scale of paracrystalline structures found in amorphous Silicon [10]. Unfortunately, it can still be difficult to obtain specifics on the formation of atomic structures in MRO with FEM alone. Collaborators have had success in using Raman spectroscopy to gain insight on the medium range order of certain glasses [11], but the method requires preexisting knowledge of which ring structures relate to spectra peaks. A computational method used for probing the MRO in atomic models is the partial pair distribution function [12], which gives the likelihood of finding pairs of specific atom types at certain pair distances, and is often used to find the most common metal-metal and metal-oxygen bond lengths in oxides. This is an easy way of identifying the existence of MRO as well as extracting the distance between atom types contained in MRO features and offering an estimate of their sizes. However, the partial PDF gives very limited insight into why pairs of atoms are more commonly found at these different distances. Ring structure analysis [13] has also been used to explain the existence of MRO in the atomic structure studies of archetypal glass silica, geramia, and boron trioxide, and work has shown a relationship between rings and mechanical loss [14].

In this paper, we present a novel method to analyze the features seen in PDFs computed from atomic models of amorphous materials. The features, in principle, could be at any distance including the medium range. The necessity of such a computational tool has been felt for a long time because of the following reason: researchers who measure or model the total PDF of amorphous materials usually have no way to systematically predict what various peaks in the PDF mean in terms of atomic structure particularly beyond 5 Å, i.e. in the medium range. However, because reliable computer models of amorphous materials can now be developed routinely, it is possible to address this limitation. In principle, these atomic models have all the information about what structures lie underneath the various features in the PDFs. Here, we present a computational tool that efficiently and systematically identifies those features.

The method of analysis presented in this paper is used, as an example, to analyze PDFs of zirconia tantala (Ta_2O_5:ZrO_2), hereafter referred to as TZO. We show that the proposed analysis enables us to identify novel features inside the structures. This is possible, because unlike other methods, this technique can give precise details on how bonds form medium range structures. We also use this technique to understand the changes seen in the PDFs due to annealing through a change in the topology of chains, where chains from annealed samples are kinkier than chains from as-deposited samples. An added benefit of this method, is that it can be very easily applied to specific distances, so one does not need to waste time with unnecessary computations, and gives the user a large amount of control not seen in the above methods. TZO has shown promise as a possible material

for the high refractive index layer in mirror coatings for future upgrades of Advanced LIGO and Advanced Virgo [15]. While this analysis focuses on MRO of TZO for its prospective use in LIGO optics (see following paragraph), the proposed computational method is versatile and can be readily extended to other amorphous materials.

Currently, gravitational-wave detectors employ alternating layers of amorphous titania-doped tantala and silica to make high quality interferometer mirrors. The thermal noise contribution from the titania-doped tantala layers is seen as a major barrier to improving the sensitivity of LIGO in its next upgrade [16]; thus a search to replace the titania-doped tantala coating has been underway. TZO is seen as a prospective coating material because under annealing, the coating has low mechanical loss [17] and the maximum annealing temperature of TZO is higher than that of pure tantala [15].

Previous work done on TZO [18] has extensively studied how annealing changes the atomic features found in TZO below 5 Å. These features include oxygen-sharing polyhedra, coordination number, bond angle distribution, and bond orientational order parameters, with the work going into great detail demonstrating how annealing TZO increases the percentage of corner-sharing polyhedra while reducing the percentage of edge and face-sharing polyhedra. The PDFs in that work also show significant differences beyond 5 Å. These as-deposited and annealed PDFs from experiments and simulations (see section II.A Computational Method), presented in Fig. 1, show peaks and troughs at various distances in the mid-range. Until now there has been no good explanation for these MRO differences.

In this work, we show that annealing TZO causes the MRO chains to increase in kinkiness through a decrease in the pair distance between end atoms. These changes occur for all metal-metal, metal-oxygen, and oxygen-oxygen chains studied in this work and explain the differences seen in the pair distribution function in the medium range. We also find that metal atoms in less kinky chains tend to have higher coordination resulting in annealed TZO having a more uniform atomic structure than as-deposited TZO. [19]. Finally, we show that there is correlation between MRO structures, where the existence of one structure is dependent on the existence of another structure.

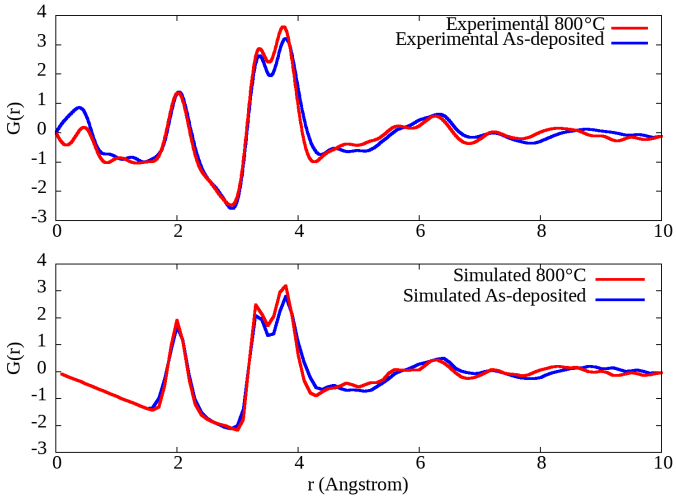

FIG. 1. The as-deposited (blue) and annealed at 800°C (red) pair distribution functions from experiment [18] (Top) and models (Bottom).

II. METHODS

A. Computational Techniques

We generated atomic models by fitting computed x-ray PDF to measured grazing-incidence PDF measurements. These measurements were carried out on films of approximately 48 percent (Zr/(Ta+Zr)) doped TZO deposited by MLD technologies through ion-beam sputtering and approximately 590 nm thickness on fused silica substrates [18]. The GIPDF data came from as-deposited samples and samples deposited under the same conditions and subsequently annealed at 800°C for 12 hours.

The models used here were created by Prasai *et al.* [18] and the entire fitting procedure was thoroughly outlined in their supplementary material [17]. For completeness though, we briefly outline the work here. 2600 atom models were first created through a melt-quench method. Then using the F.E.A.R. method [20], models were iterated between Reverse Monte Carlo (RMC) and energy minimization with molecular dynamics. To ensure the correctness of these models, bond length distributions from smaller *ab inito* molecular dynamics simulations were used to constrain the RMC interactions. With this method 2000 models were made, with 1000 being from as-deposited measurement data and the other being from annealed at 800°C measurement data. The PDFs from these models are shown in Fig. 1 and clearly capture the same PDF features from experiment [18].

The technique used here to probe the MRO was performed with a method from graph theory that enables the study of structures of arbitrary lengths. The process begins by turning all atoms into nodes and all metal-oxygen (M-O) bonds, using a cutoff of 2.9 Å, into edges weighted by distance, to make a graph [21]. The Djikstra algorithm [22] is then used to find the shortest paths connecting all pairs of atoms. For simplicity, each path of atoms is called a chain, which can then be categorized by what distance their ending atoms are from each other. Examples of these chains can be seen in Fig. 2 and Fig. 7. This allows for the identification of structures that connect any pair of atoms, which is ideal for examining the PDF, since the PDF tells the likelihood of finding pairs of atoms specific distances apart. Here we focus on the distances between 3.1-9.9 Å.

B. N-Metal Chains

We find it convenient to describe the chains in disordered materials in terms of a) the number of metals involved and b) their kinkiness. These two descriptors determine the length of the chain i.e. their contribution in different length scales at g(r). Examples of different N-metal chains can be seen in Fig. 2, which contains 3, 4, and 5 metal chains. When comparing chains involving the same number of metal and oxygen atoms, the kinkier chains tended to be shorter. We chose these metrics so chains can easily be used to study the pair distribution function.

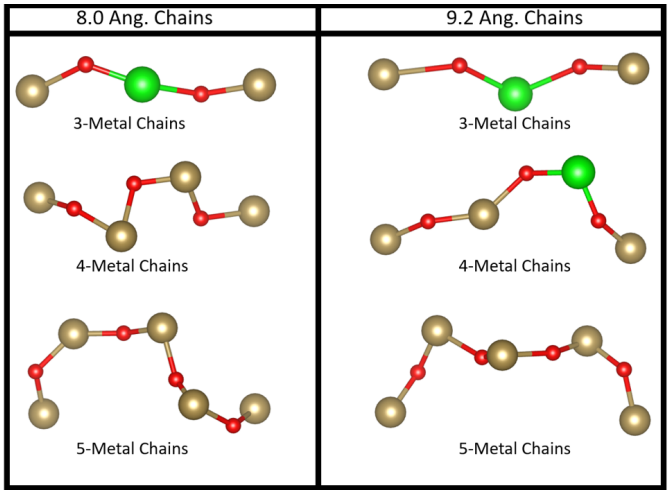

FIG. 2. Examples of N-metal chains for 8.0 Å and 9.2 Å pair distances. Red atoms are oxygen, gold atoms are tantala, and green atoms are zirconia.

III. RESULTS

A. N-Metal Chains

To study the general effect annealing has on MRO, we calculated the percent and average number of N-metal chains that connect metal atoms at distances between 3.1 and 9.9 Å, shown in the top of Fig. 3 and Fig. 4 for the as-deposited (dashed) and annealed (solid) models. This calculation was performed by using our methodology to identify all metal-metal chains at specific pair distances and then classifying them by the number of metals in the chain. Fig. 3 shows that chains are predominantly made of 1 or 2 different N-metal chains. Specifically, it is observed in metal-metal chains that have pair distances between 3 Å and 4.5 Å, 2-metal chains are predominant, between 4.5 Å and 7.5 Å 3-metal chains are predominant, and beyond 7.5 Å, 4 or more metal chains are predominant. Our method allowed us to not just predict these relationships based on the present interatomic potentials but precisely quantify them.

The interatomic potentials [23, 24] governing the systems' atoms are the prominent reason that these chains are found within the aforementioned distances. Previous Ab-initio molecular dynamics calculations [17] show tantala-oxygen bond lengths are typically between 1.5 and 2.9 Å, while zirconia-oxygen bond lengths are typically between 1.5 and 3.2 Å. As the lengths of metal-oxygen bonds approach either of these extremes the energies on participating atoms become less realistic. This is illustrated by Fig. 5 where the average energy per atom of the chains is plotted, as the chains' terminal atoms' pair distances become too large or small their energies increase. For clarity, in Fig. 5, we have elected to only plot energies for N-metal chains at pair distances where the number of chains at that pair distance is at least .01 percent between 3.1 and 9.9 Å. Fig. 5 exhibits that below 4.5 Å 2-metal chains have their lowest energy. Meanwhile, the 3-metal chains have lower energies compared to 4-metal chains til their pair distances are greater than approximately 6.2 Å, at which point the absolute difference in the average energy per atom between the 3-metal chains and 4-metal chains first decreases and then sharply increases after 7.5 Å. This sharp increase means TZO coatings have a larger and increasing proportion of 4-metal chains compared to 3 metal chains when the chains' pair-distances are beyond 7.5 Å.

Therefore, with this method we very easily gained insight on the atomic scale of the MRO structures and the types of chains that make them. For example, we can say the peak near 5 Å is created by an abundance of 3-metal chains. This will help us better understand the correlated structures we see in the final section.

When comparing the annealed distributions (solid) to the as-deposited distributions (dashed) in Fig. 3 and Fig. 4, we clearly see that the as-deposited lines are always to the right of the annealed lines, even though the bond lengths of the two samples are the same. This demonstrates that annealing TZO decreases the pair distances of the chains' terminal atoms. This could only happen by having the chains be built out of shorter bonds at all distances, or they have become kinkier. We will show in the section III.B, that the chains have indeed become kinkier. This result represents an understandable change in the MRO due to annealing, that can help theorists and experimentalists alike better comprehend the topological underpinnings of the PDF differences. This is also of particular significance as tantala and tantala doped films undergoing post-deposition annealing show a consistent change in PDF at this distance [1, 18, 25] and could also mean that an increase in kinkiness of MRO chains may be responsible for lowering room temperature mechanical loss. We also see in the middle and bottom of Fig. 3 that this trend holds for M-O and O-O chains as well.

Fig. 4 shows that each N-metal chain has an obvious distance where that chain type is most common. For 3-metal chains this is near 6.2 Å; for the 4-metal chains the distance is near 9 Å. Chains whose pair distances are

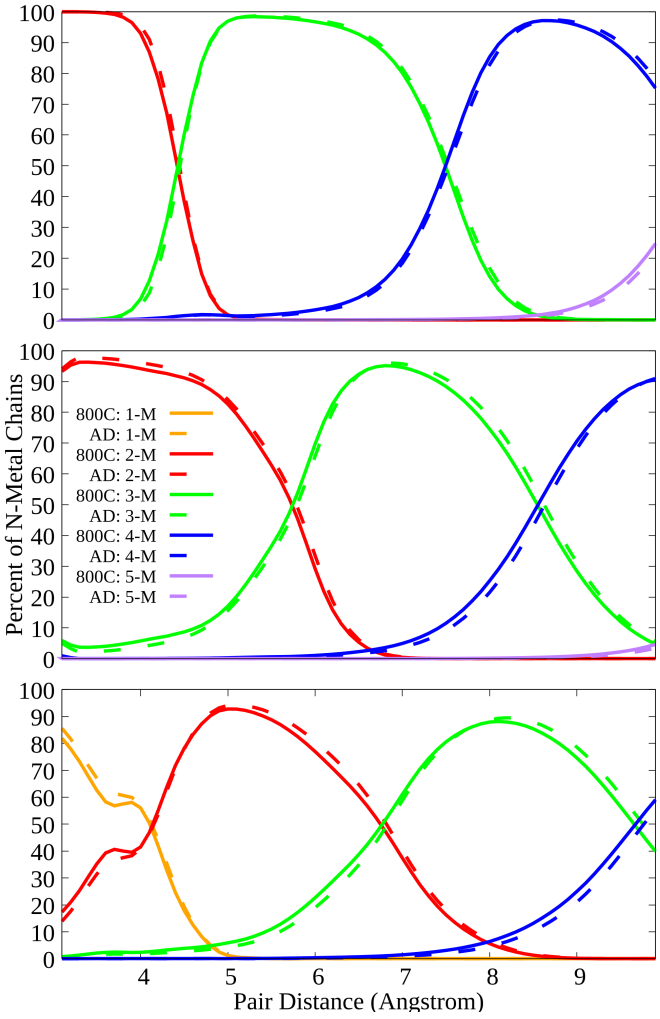

FIG. 3. (Top) Percent of N-metal chains which connect metal atoms found at pair distances from 3.1-9.9 Å. (Middle) Percent of N-metal chains which connect metal to oxygen atoms found at pair distances from 3.1-9.9 Å. (Bottom) Percent of N-metal chains which connect oxygen atoms found at pair distances from 3.1-9.9 Å. Solid lines are the percent of chains from models of samples annealed at 800°C and dashed lines are from models of as-deposited samples.

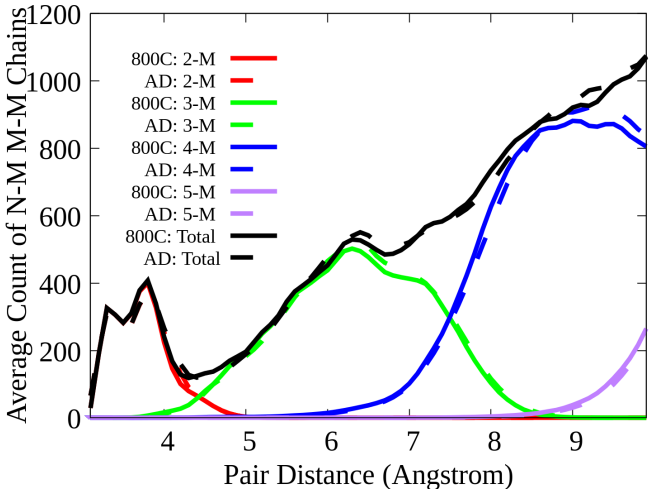

FIG. 4. The average count of N-metal chains that connect metal to metal atoms found at pair distances from 3.1-9.9 Å. Solid lines are from models of samples annealed at 800°C and dashed lines come from the models of as-deposited samples. The black lines are the average total number of all metal-metal chains.

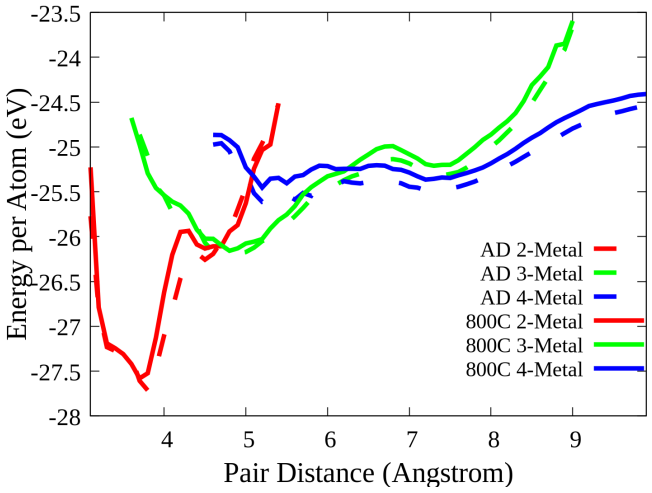

FIG. 5. Average energy of N-metal chains which connect metal atoms found at pair distances from 3.1-9.9 Å. If the number of N-metal chains which connect metal atoms found at a pair distance was less than .01 percent the total number of the same type of chains from 3.1-9.9 Å, then the average energy was not plotted at that distance.

smaller than these peak locations will be kinkier than those with a larger pair distance. Under this definition, Fig. 4 exhibits that MRO regions where the annealed PDF is larger than the as-deposited PDF come from kinkier chains. For example, region 4.7 - 5.7 Å and region 7.2 - 8.5 Å, have more annealed than as deposited pairs, as seen in the PDF, which come from the kinkier 3-metal chains and the kinkier 4-metal chains respectively. We will describe kinkiness in detail in section III.B.

B. Kinkiness

As mentioned in the previous section, the chains present in annealed at 800°C TZO have terminal atoms closer to each other than the chains present in as-deposited TZO of the same type even though the metal-oxygen peak near 2 Å in Fig. 1 does not significantly change during annealing. Thus, we argue in this section that the differences seen in Fig. 4 and the MRO of Fig. 1 are due to how these chains are constructed, specifically how kinky they are. To better demonstrate this point, we develop a simple formula for defining the kinkiness of chains as the total perpendicular distance inner atoms are from the pair distance vector connecting terminal atoms,

as shown in equations 1 through 3. T_1 is the position of one terminal atom, T_2 is the position of the other terminal atom, and M_i is the position of inner atom i.

$$\hat{r} = \frac{T_1 - T_2}{|T_1 - T_2|} \tag{1}$$

$$\theta_i = \arccos \frac{T_1 - M_i}{|T_1 - M_i|} \cdot \hat{r} \tag{2}$$

$$K = \sum_i |T_1 - M_i| \sin(\theta_i) \tag{3}$$

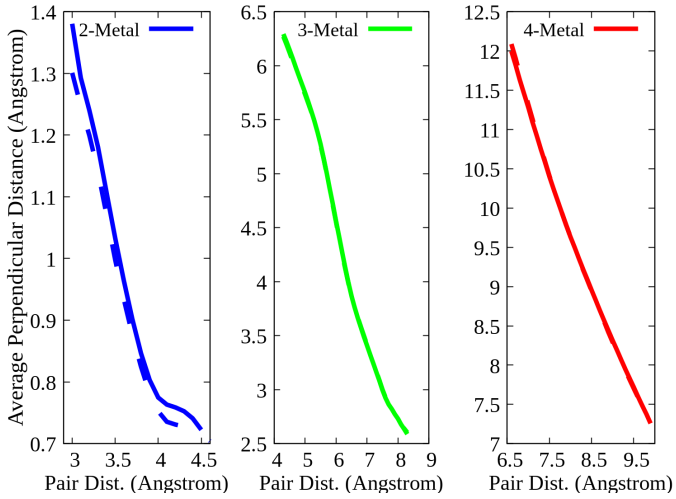

FIG. 6. (Left) The average kinkiness of 2-metal chains which connect metal atoms. (Middle) The average kinkiness of 3-metal chains which connect metal atoms. (Right) The average kinkiness of 4-metal chains which connect metal atoms

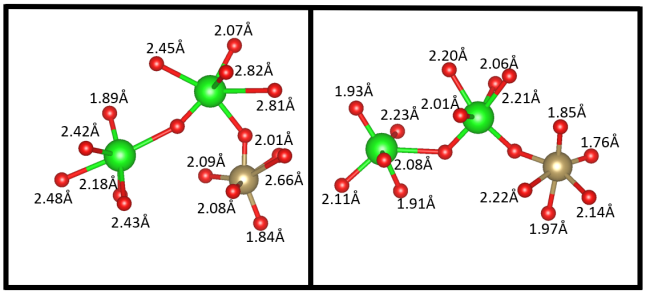

FIG. 7. (Left) A 3-metal chain which connects terminal atoms 5 Å apart and has a kinkiness of 6.45 Å. The neighboring oxygen and their distances from the metal atoms are included. (Right) A 3-metal chain which connects terminal atoms 7 Å apart and has a kinkiness of 2.55 Å. The neighboring oxygen and their distances from the metal atoms are included.

Fig. 6 shows that as the distance between terminal metal atoms decreases the kinkiness increases. Since the pair distances of the terminal atoms in annealed at 800°C chains are shorter than the pair distances of the terminal atoms in as-deposited chains, annealing TZO must increase the kinkiness of the chains present.

As a chain becomes kinkier, the neighboring oxygen atoms move father away from the chain. An example of this can be seen in Fig. 7, where the oxygen neighboring the 5 Å chain are father away from the chain compared to the oxygen neighboring the 7 Å chain. To further illustrate this point the average coordination number of the 2-metal, 3-metal, and 4-metal chains versus pair distance are plotted in Fig. 8. Again, we have elected to only plot coordination values for N-metal chains at pair distances where the number of chains at that pair distance is at least .01 percent the total number of N-metal chains between 3.1 and 9.9 Å. We see that the less kinky chains have a higher coordination number, which is consistent with previous work performed by [19] that showed annealing TZO decreases the overall coordination number of the coatings. Consequently, since the density of the experimental samples did not change during the annealing process (confirmed with a combination of Areal Density, thickness, and composition measurements [17]), the larger proportion of kinkier chains in the annealed at 800°C models results in more uniform atomic structures which also explains the smaller voids seen in [19]. The findings that voids are annihilated when chains become kinkier due to annealing is an interesting result that runs contrary to observations made on nanopores [26, 27] . Anghinolfli et al observe that annealing causes the pore density of oxide optical coatings to increase, while Stenzel et al find that pores are necessary to reduce compressive strain. There are of course many scenarios where these and our finding can be consistent. For example, in a scenario where density is not fixed, chains could become kinkier while still allowing pores to increase in size. To find out if this is the case more work with larger models and different materials is needed.

C. Zirconia Proportion

One aspect of this research that may interest the scientific community at large is how changing doping percentages may affect the kinkiness of TZO coatings. We have calculated the average kinkiness of chains (equations 1-3) whose terminal atoms are both metals versus the percentage of zirconia metals found in 2-metal, 3-metal, and 4-metal chains. The results are presented in Fig. 9. It is clear that as the percentage of zirconia increases in the chains the kinkiness of the chains increases as well. The only N-metal chains not following this trend are 4-metal chains found in the as-deposited models. However, that result does not account for all 4-metal chains in TZO since our 9.9 Åcut off limits us from including longer 4-metal chains in our analysis, which could affect the results. From the 2-metal and 3-metal chain results it is apparent that increasing or decreasing the doping per-

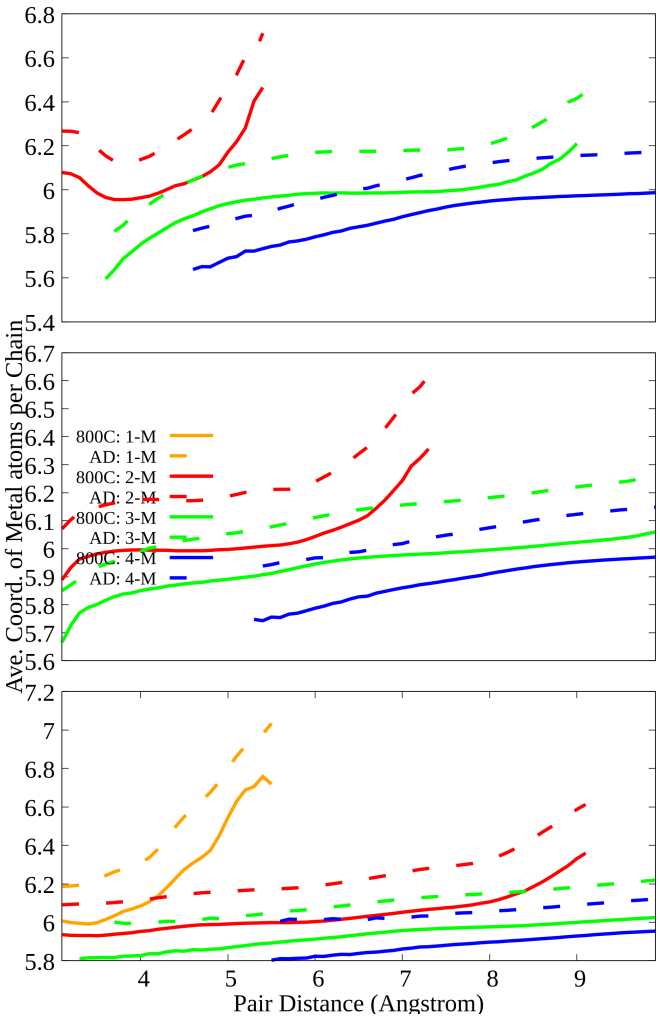

FIG. 8. (Top) Average coordination number of metal atoms in N-metal chains which connect metal atoms found at pair distances from 3.1-9.9 Å. (Middle) Average coordination number of metal atoms in N-metal chains which connect metal to oxygen atoms found at pair distances from 3.1-9.9 Å. (Bottom) Average coordination number of metal atoms in N-metal chains which connect oxygen atoms found at pair distances from 3.1-9.9 Å. Solid lines are for the average coordination from models of samples annealed at 800°C and dashed lines are from models of as-deposited samples. The average coordination number for a specific chain type was only plotted at a specific pair distance if the number of chains at that specific distance was at least .01 percent of the total number of chains of the same type.

centage of zirconia will increase or decrease the overall kinkiness of TZO.

D. Correlating Pair Distribution Function Peaks

The most unexpected insight gained through this novel technique is the identification of hidden structure inside the PDF. For example, we find that several peaks in

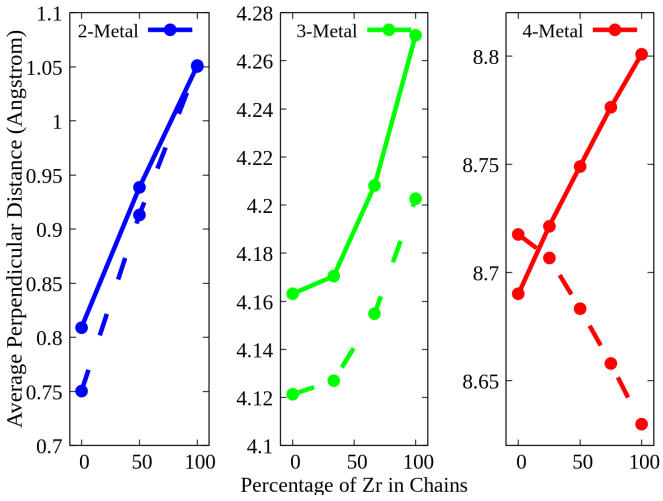

FIG. 9. (Left) The average kinkiness of 2-metal chains which connect metal atoms versus the percent of zirconia metals in those chains. (Middle) The average kinkiness of 3-metal chains which connect metal atoms versus the percent of zirconia metals in those chains. (Right) The average kinkiness of 4-metal chains which connect metal atoms versus the percent of zirconia metals in those chains. Annealed at 800°C results are represented by solid lines and as-deposited results are represented by dashed lines

the PDF at medium range are correlated, *i.e.* these, although few Angstroms apart, are manifestations of the same chain. Here, we demonstrate this phenomenon by analyzing the composition of peaks at higher distances. We also introduce the concept of sub-chains, which are chains that are a part of larger chains.

To be specific, we use functions from the seaborn library [28] to perform kernel density estimations (KDEs), of all metal-metal distances (pair distances of sub-chain end atoms) that are part of the metal-metal 5.1, 6.8, 8.0, and 9.2 Å chains. The distances between end atoms were not included, as this analysis focuses only on constituent parts. These results, Fig. 10, contain very different KDEs depending on the distance under investigation, however differences due to annealing are negligible.

9.2 Å and 8.0 Å chains have the most distinct distributions of the studied set, with the most obvious differences occurring at 5.2 and 6.1 Å . The lack of sub-chains found at 5 Å in the 9.2 Å chain is fascinating, as it implies there is little to no correlation between 9.2 Å chains and 5 Å chains. Thus, when TZO is annealed and the number of 5 Å chains are increased, the 8 Å chains increases with them, while the 9.2 Å chains will remain mostly unaffected. This correlation can be explained by the idea that larger chains are dependent upon the availability of smaller sub-chains. The presence or absence of sub-chains will then affect the presence or absence of their larger chains, and consequently peaks derived from these two different chains will be inextricable.

The absence of 5 Å sub-chains in 9.2 Å chains may seem odd at first but upon inspection of Fig. 3 the rea-

son becomes abundantly clear. A 5 Å chain will most likely be made out of a 3-metal chain. Meanwhile, a 9.2 Å chain is usually made out of 4-metal chains. If a 9.2 Å chain contained a 5 Å sub-chain, then that chain would need to contain a 2-metal sub-chain with a pair distance greater than 4.2 Å. There are very few 2-metal chains that meet these requirements, and so there is a large valley near 5 Å in Fig. 10. Compare this to the 8 Å chain. 8 Å chains, similar to 9.2 Å chains, are mostly 4-metal chains. However, if the 8 Å chain contains a 5 Å chain, then it will only need a 2-metal chain with a distance greater than 3 Å, which is very common. This also explains why the 8 Å KDE has a large spread near 5 Å. Hence, the difference in the distribution functions of the 9.2 Å and 8 Å chains is very easy to understand once the common N-metal chains are known for these distances. Therefore, large MRO structures are constrained by the distribution of the smaller structures inside them.

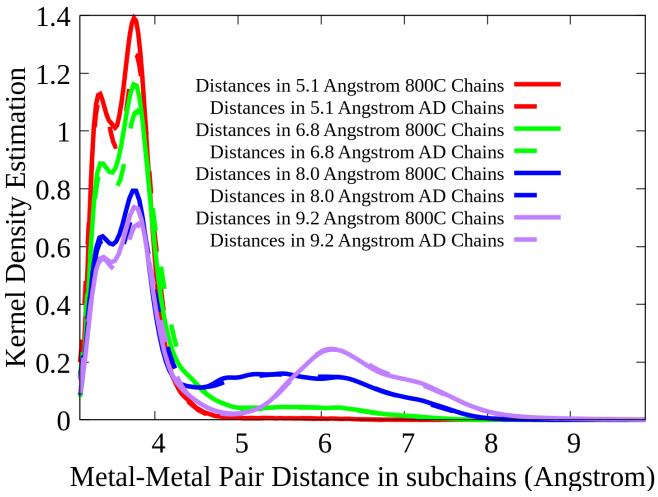

FIG. 10. Distribution of pair distances from metal-metal subchains found in 5.1, 6.8, 8.0, and 9.2 Å chains from as-deposited (solid) and 800°C (dashed). The end metal distances were not included.

IV. CONCLUSIONS AND DISCUSSIONS

In this work we introduced a new computational tool that is both easy to use and gives significant information about the medium range order. The method itself can be applied to any model, and can be used to investigate MRO features found in the PDF at arbitrary lengths.

For our analysis, the FEAR method was used to generate atomic models of amorphous zirconia-tantala, by creating 2000 models fit to two sets of experimental GIPDF data. Both the experimental and simulated PDF demonstrated significant differences well into the medium range order that had not been explained until now. With our new computational tool we were able to explain that the differences seen in the medium range order come from an increase in the kinkiness of chains when the films are annealed. The fact that the annealed chains were kinkier suggests kinkiness may affect room temperature elastic dissipation and should be furthered studied. These findings give more information to the community developing low-thermal-noise mirrors for interferometric gravitational-wave detectors and others interested in the mechanisms responsible for elastic dissipation in amorphous solids.

We also demonstrated that medium range order peaks found in the PDF are correlated. We were able to explain this correlation through the existence of sub-chains, and how these sub-chains must exist for larger chains to exist as well.

ACKNOWLEDGMENTS

The work is supported by NSF/PHY 1707870, NSF/PHY 1707964, PHY 1404110, and UF Informatics Institute Graduate Fellowship. Computations were done using the utilities of the National Energy Research Scientific Computing Center and the University of Florida's hipergator.We acknowledge the support of the LSC Center for Coatings Research, jointly funded by the National Science Foundation (NSF) and the Gordon and Betty Moore Foundation (GBMF). In particular, the authors are grateful for support through NSF awards PHY-1707866, PHY-1708175, and GBMF Grant No. 6793. Partial support from grant ONR No. N00014-17-1-2536 is acknowledged. We would like to thank the Sherlock Cluster at Stanford University for providing computational resources and support that contributed to these research results. This work also used the Extreme Science and Engineering Discovery Environment (XSEDE) [76], which is supported by National Science Foundation grant number ACI-1548562

[1] M. J. Hart, R. Bassiri, K. B. Borisenko, M. Véron, E. F. Rauch, I. W. Martin, S. Rowan, M. M. Fejer, and I. MacLaren, Medium range structural order in amorphous tantala spatially resolved with changes to atomic structure by thermal annealing, Journal of Non-Crystalline Solids **438**, 10 (2016).
[2] Y. Pan, F. Inam, M. Zhang, and D. Drabold, Atomistic origin of Urbach tails in amorphous silicon, Physical review letters **100**, 206403 (2008).
[3] D. Drabold, Y. Li, B. Cai, and M. Zhang, Urbach tails of amorphous silicon, Physical Review B **83**, 045201 (2011).
[4] A. Amato, S. Terreni, M. Granata, C. Michel, L. Pinard, G. Gemme, M. Canepa, and G. Cagnoli, Effect of heating treatment and mixture on optical properties of coating

materials used in gravitational-wave detectors, Journal of Vacuum Science & Technology B, Nanotechnology and Microelectronics: Materials, Processing, Measurement, and Phenomena **37**, 062913 (2019).

[5] A. Amato, S. Terreni, M. Granata, C. Michel, B. Sassolas, L. Pinard, M. Canepa, and G. Cagnoli, Observation of a correlation between internal friction and Urbach energy in amorphous oxides thin films, Scientific reports **10**, 1 (2020).

[6] A. Sokolov, A. Kisliuk, M. Soltwisch, and D. Quitmann, Medium-range order in glasses: Comparison of Raman and diffraction measurements, Physical review letters **69**, 1540 (1992).

[7] R. Holomb, V. Mitsa, E. Akalin, S. Akyuz, and M. Sichka, Ab initio and Raman study of medium range ordering in GeSe2 glass, Journal of non-crystalline solids **373**, 51 (2013).

[8] P. Voyles and D. Muller, Fluctuation microscopy in the STEM, Ultramicroscopy **93**, 147 (2002).

[9] J. J. Maldonis, J. Hwang, and P. M. Voyles, FEMSIM + HRMC: Simulation of and structural refinement using fluctuation electron microscopy for amorphous materials, Computer Physics Communications **213**, 217 (2017).

[10] J. Gibson, M. Treacy, T. Sun, and N. Zaluzec, Substantial crystalline topology in amorphous silicon, Physical review letters **105**, 125504 (2010).

[11] L. Yang, G. Vajente, M. Fazio, A. Ananyeva, G. Billingsley, A. Markosyan, R. Bassiri, K. Prasai, M. M. Fejer, M. Chicoine, *et al.*, Enhanced medium-range order in vapor-deposited germania glasses at elevated temperatures, Science Advances **7**, eabh1117 (2021).

[12] B. Aoun, Fullrmc, a rigid body reverse monte carlo modeling package enabled with machine learning and artificial intelligence, Journal of computational chemistry **37**, 1102 (2016).

[13] S. Le Roux and P. Jund, Ring statistics analysis of topological networks: New approach and application to amorphous GeS2 and SiO2 systems, Computational Materials Science **49**, 70 (2010).

[14] M. Granata, E. Coillet, V. Martinez, V. Dolique, A. Amato, M. Canepa, J. Margueritat, C. Martinet, A. Mermet, C. Michel, *et al.*, Correlated evolution of structure and mechanical loss of a sputtered silica film, Physical Review Materials **2**, 053607 (2018).

[15] M. Abernathy, A. Amato, A. Ananyeva, S. Angelova, B. Baloukas, R. Bassiri, G. Billingsley, R. Birney, G. Cagnoli, M. Canepa, *et al.*, Exploration of co-sputtered Ta2O5-ZrO2 thin films for gravitational-wave detectors, Classical and Quantum Gravity **38**, 195021 (2021).

[16] G. M. Harry, A. M. Gretarsson, P. R. Saulson, S. E. Kittelberger, S. D. Penn, W. J. Startin, S. Rowan, M. M. Fejer, D. Crooks, G. Cagnoli, *et al.*, Thermal noise in interferometric gravitational wave detectors due to dielectric optical coatings, Classical and Quantum Gravity **19**, 897 (2002).

[17] K. Prasai, J. Jiang, A. Mishkin, B. Shyam, S. Angelova, R. Birney, D. Drabold, M. Fazio, E. Gustafson, G. Harry, *et al.*, Supplementary information-High precision detection of change in intermediate range order of amorphous zirconiadoped tantala thin films due to annealing, Physical review letters (2019).

[18] K. Prasai, J. Jiang, A. Mishkin, B. Shyam, S. Angelova, R. Birney, D. Drabold, M. Fazio, E. Gustafson, G. Harry, *et al.*, High precision detection of change in intermediate range order of amorphous zirconia-doped tantala thin films due to annealing, Physical review letters **123**, 045501 (2019).

[19] R. Thapa, K. Prasai, R. Bassiri, M. M. Fejer, and D. Drabold, Realistic computer models of amorphous ZrO2:Ta2O5: Structural, optical, and vibrational properties, Physical Review B **105**, 224207 (2022).

[20] A. Pandey, P. Biswas, and D. A. Drabold, Inversion of diffraction data for amorphous materials, Scientific reports **6**, 33731 (2016).

[21] M. Bóna, *A walk through combinatorics: an introduction to enumeration and graph theory* (World Scientific, 2002).

[22] A. Bhargava, *Grokking Algorithms: An illustrated guide for programmers and other curious people* (Simon and Schuster, 2016).

[23] J. Trinastic, R. Hamdan, Y. Wu, L. Zhang, and H.-P. Cheng, Unified interatomic potential and energy barrier distributions for amorphous oxides, The Journal of Chemical Physics **139** (2013).

[24] J. Yu, R. Devanathan, and W. J. Weber, Unified interatomic potential for zircon, zirconia and silica systems, Journal of Materials Chemistry **19**, 3923 (2009).

[25] B. Shyam, K. H. Stone, R. Bassiri, M. M. Fejer, M. F. Toney, and A. Mehta, Measurement and modeling of short and medium range order in amorphous Ta2O5 thin films, Scientific reports **6**, 32170 (2016).

[26] L. Anghinolfi, M. Prato, A. Chtanov, M. Gross, A. Chincarini, M. Neri, G. Gemme, and M. Canepa, Optical properties of uniform, porous, amorphous Ta2O5 coatings on silica: temperature effects, Journal of Physics D: Applied Physics **46**, 455301 (2013).

[27] O. Stenzel, S. Wilbrandt, N. Kaiser, M. Vinnichenko, F. Munnik, A. Kolitsch, A. Chuvilin, U. Kaiser, J. Ebert, S. Jakobs, *et al.*, The correlation between mechanical stress, thermal shift and refractive index in HfO2, Nb2O5, Ta2O5 and SiO2 layers and its relation to the layer porosity, Thin Solid Films **517**, 6058 (2009).

[28] M. Waskom and the seaborn development team, mwaskom/seaborn (2020).